# Magnetoelectricity of domain walls of rare-earth iron garnets

A. I. Popov,[1,2] Z. V. Gareeva,[3,4,*] and A. K. Zvezdin[1,5,6]

[1]*Moscow Institute of Physics and Technology (State University), 141700, Dolgoprudny, Russia*
[2]*National Research University of Electronic Technology, 124498, Zelenograd, Moscow, Russia*
[3]*Institute of Molecule and Crystal Physics, Russian Academy of Sciences, 450075, Ufa, Russia*
[4]*Bashkir State University, 450076, Ufa, Russia*
[5]*A.M. Prokhorov General Physics Institute, Russian Academy of Sciences, 119991, Moscow, Russia*
[6]*P.N. Lebedev Physical Institute of the Russian Academy of Sciences, 119991, Moscow, Russia*

(Received 4 June 2015; revised manuscript received 1 September 2015; published 20 October 2015)

We investigate a type of magnetoelectric effect in rare-earth iron garnets related to the presence of domain walls of the iron subsystem. The lack of space inversion in the dodecahedral rare-earth ion environments allows ferroelectric ordering in these materials. Electric polarization is absent in single-domain samples due to the antiferroelectricity of the electric-dipole structure. We show that the magnetic domain walls of the iron subsystem generate an effective inhomogeneous magnetic field arising from the rare-earth iron exchange interaction, which leads to emergence of electric polarization. A hallmark of this effect is that magnetoelectricity is independent of the type of magnetic domain walls. In contrast to the accepted concepts, we argue that the electric polarization in rare-earth iron garnets also occurs in the vicinity of Bloch magnetic walls. Magnetoelectric properties are inherent to rare-earth iron garnets in the presence of magnetic domain structure in any temperature range. Rare-earth iron garnets refer to multiferroics with $d$ and $f$ interacting subsystems.

DOI: 10.1103/PhysRevB.92.144420 PACS number(s): 75.85.+t, 75.50.Gg, 75.60.Ch

## I. INTRODUCTION

Domain walls in multiferroics have attracted a considerable attention because of multiple functionalities provided by the interplay between several ferroic parameters. The past years have witnessed a series of bright discoveries in the physics of domains. It has been found that domain walls in ferroelectrics produce charges [1–5] and generate photovoltage [6]; magnetic domain walls in superconductor-ferromagnet hybrids host superconductivity [7]; ferroelectric domain walls in multiferroics provide magnetization [8–11] and, vice versa, magnetic domain walls serve as sources of polarization [12–18].

The idea of Nobel laureate Herbert Kroemer "... that the interface is the device" also applies to domain walls [19] particularly in multiferroics. The finite dimensions, intrinsic structure, and mobility of domain walls are attractive properties for nanoelectronic implementations. With the oxide nanoelectronics on the rise, the search for novel multiferroics, the investigation of ferroelectricity, and the nature of magnetism become the subjects of fundamental and practical importance.

In typical multiferroics (bismuth ferrite, boracites, manganites), magnetoelectricity is related to odd configurations of magnetic moments of the $d$ ions (Fe, Mn, Cr). Recently, there has been an increased interest to rare-earth multiferroics where magnetoelectricity has found to be linked to the rare-earth subsystem. Representatives of the novel multiferroics are rare-earth orthoferrites [20–22]. Their magnetic moments are determined by exchange interaction between the rare-earth ($f$) and the iron ($d$) magnetic sublattices, and electric properties are related to central-asymmetrical ordering of the $f$ sublattice modes. The iron sublattice in these compounds is centrosymmetrical, hence magnetoelectrically inactive, and the magnetic moments of the rare-earth ions can in turn be ordered into asymmetrical, spatially odd modes, which results in the appearance of the spontaneous electric polarization. Magnetoelectric effects and anomalies of the electric polarization in rare-earth orthoferrites were predicted theoretically and investigated experimentally in Refs. [21,22]. The magnetoelectric properties of these magnets are sensitive to the type of antiferromagnetic ordering and to the orientation of the $d$ ion spins.

The rare-earth iron garnets can also be classified as novel multiferroics since their rare-earth subsystem is subjected to the exchange rare-earth–iron interaction. Unlike orthoferrites in iron garnets, the $f$-$d$ exchange coupling induces an antiferroelectric structure [18]. In this regard, we are interested in exploring their magnetoelectric properties. The magnetoelectric effect in iron garnets was known from the work of O'Dell [23], see also Refs. [23–26] exploring quadratic in electric field effects. The quadratic magnetoelectric effect is allowed by the symmetry of iron garnets. The works [15,27–32] reported a linear magnetoelectric effect in films and crystals of these compounds. The origin of such effects in the iron garnet crystals still remains a puzzle, which stimulates ongoing experimental and theoretical studies of these phenomena [12,14–18,33–37].

In our paper, we report a type of magnetoelectricity in rare-earth iron garnets that caused by domain structure. We argue that domain walls can be considered as a source of an effective inhomogeneous exchange field that acts on the rare-earth ions and leads to electric polarization. The essence of this effect is as follows. The rare-earth ions occupy in the garnet structure 12 nonequivalent positions, which have no inversion center. In a uniform magnetic (or exchange) field, they acquire electric dipole moments which are oriented in different directions (Fig. 1). Thus, according to the symmetry, the total dipole moment as a result of summation over the positions vanishes. However, in an inhomogeneous field, the strict compensation of local dipoles is disturbed. This results in a total electric dipole moment of the crystal. Its magnitude and direction are determined by the exchange field gradient created by the domain wall.

*gzv@anrb.ru

 

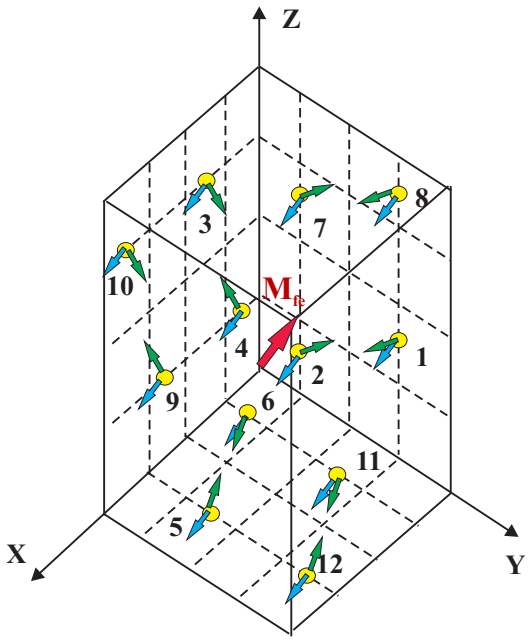


FIG. 1. (Color online) The structure of the magnetic and the electric-dipole moments of $Eu^{3+}$ ion in the primitive cell of $Eu_3Fe_5O_{12}$. The red arrow shows the direction of intrinsic magnetic field related to $M_{Fe}$. The blue arrows correspond to the magnetic moments of $Eu^{3+}$ ion and the green arrows correspond to the electric-dipole moments of $Eu^{3+}$ ion.

This effect drastically differs from the well-known magnetoelectric effects related to domain walls and cycloids in multiferroics, which according to Refs. [13,38] are forbidden by the symmetry of Bloch domain walls. We show that due to the rare-earth iron exchange interaction a nonzero magnetoelectric effect in iron garnets can be realized in all types of domain walls (Bloch, Neel, and others) in all temperature ranges.

The magnitude of the effective magnetic field in rare-earth iron garnets is about $10^{-3}$ T. An estimation of the polarization induced by the effective field in garnets gives a value around 10–100 $\mu\,C/m^2$ (if one supposes that domain walls of the same chirality occupy 1%–5% of the crystal volume and the exchange field of the rare-earth iron subsystems is $H_{ex} \approx$ 10–20 T); for comparison, in ferroborates, the magnitude of the exchange field is $H_{ex} \approx 5$ T and polarization attains values around [39] 100–400 $\mu\,C/m^2$.

## II. CRYSTAL STRUCTURE OF RARE-EARTH IRON GARNETS

A family of rare-earth compounds with garnet structure for decades remains the subject of intensive investigations because of the number of unique magnetic, magnetoelastic, and magnetooptical properties appearing in most cases due to the presence of the rare-earth ions [40,41]. A rare-earth garnet has the chemical formula $R_3M_5O_{12}$, where $R$ stands for a rare-earth or yttrium ion and $M$ stands for a metal ion, which can be divalent ($Co^{2+}$,$Ga^{2+}$,$Mn^{2+}$,$Fe^{2+}$,$Ni^{2+}$), trivalent ($Fe^{3+}$,$Ga^{3+}$,$Al^{3+}$, $Se^{3+}$,$V^{3+}$,$Cr^{3+}$), tetravalent ($Ge^{4+}$,$Si^{4+}$,$Zn^{4+}$,$Ni^{4+}$,$Sn^{4+}$), and pentavalent ($Nb^{5+}$,$P^{5+}$,$As^{5+}$). Commonly, garnet crystals are divided into magnetic garnets whose $M$ ions belong to the transition metal group with an unfilled $d$ subshell and nonmagnetic garnets with $Al^{3+}$,$Ga^{3+}$,$Ge^{4+}$, and $S^{4+}$ $M$ ions. The garnet structure provides wide possibilities that could be attained by the substitution of different ions (both magnetic and nonmagnetic), one on the others. The rare-earth garnets are cubic magnets having complicated crystallographic structure, described by the $O_h^{10}$-$Ia3d$ space group. Their body centered cubic unit cell contains eight formula units, namely, 160 atoms. Its lattice parameter (the cell edge length) $a \approx 12$ Å. It is of importance that the rare-earth ions in the garnet crystals are located in six crystallographically inequivalent positions whose symmetry is lower than the cubic one. The symmetry of the rare-earth ion environment in garnets is described by the $D_2$ point group, in which the space inversion operation is lacking. It is the basic point that allows us to understand the magnetoelectricity of garnets [18]. To elucidate the physical properties of rare-earth iron garnets, it is sufficient to consider the primitive cell, which is twice smaller than the unit cell and contains four $R_3M_5O_{12}$ units. The coordinates of all 12 rare-earth ions in the primitive cell and the orientation of their local symmetry axes are given in the Table I taken from Ref. [18]. The numbering of the rare-earth ion positions in a primitive cell is chosen in such a way that the $(k+6)$-th position ($k = 1,\ldots,6$) differs from the $k$th position by the inversion operation, which is equivalent to the relation $\boldsymbol{e}_y^{(k+6)} = -\boldsymbol{e}_y^{(k)}$ (see the Table I [18]).

The lack of space inversion in the rare-earth ion environment leads to induction of the electric-dipole moment of the rare-earth ion and as a consequence to the appearance of the electric-dipole structure of a crystal [18]. However, in the presence of a homogeneous magnetic field, the total electric-dipole moment derived as a result of the summation over all positions of the rare-earth ions in the primitive garnet cell vanishes due to the inversion operation coupling the $k$th and the $(k+6)$-th positions. The nonzero electric-dipole moment of the cell may arise either in the garnet films, or in the case of an inhomogeneous magnetic field acting on the rare-earth ions, as was shown in Ref. [18]. The appearance of polarization in an artificial inhomogeneous magnetic field $\boldsymbol{H} = \boldsymbol{n}(\boldsymbol{n}\cdot\boldsymbol{r})$, where $\boldsymbol{n}$ is the unit vector determining the direction of the change of the magnetic field ($\nabla\boldsymbol{H}$) was demonstrated in Ref. [18]. The presence of a domain wall in rare-earth iron garnets is a natural opportunity to implement the effective inhomogeneous magnetic field acting on the rare-earth ions by the iron ions. It should be mentioned that the magnetoelectric properties of domain walls were discussed in Refs. [13,38]. In particular, the authors of Ref. [38] state that electric polarization can arise in the vicinity of Neel-like domain walls, and the emergence of an electric polarization of the Bloch domain walls is impossible. We show the possibility of magnetoelectricity in the rare-earth subsystem attributed to the inhomogeneous effective magnetic field of the exchange rare-earth iron interaction generated by Bloch and Neel domain walls.

## III. MAGNETOELECTRIC INTERACTIONS AND ANTIFERROELECTRIC STRUCTURE OF RARE-EARTH IRON GARNETS

The expression for the operator of rare-earth ion magnetoelectric interaction $H_{me}$ in the garnet crystal has been deduced

TABLE I. The coordinates and the symmetry axes of the dodecahedral $c$ positions.

| $k$ | 1 | 2 | 3 | 4 | 5 | 6 | 7 | 8 | 9 | 10 | 11 | 12 |
|---|---|---|---|---|---|---|---|---|---|---|---|---|
| $\boldsymbol{r}^{(k)}$ | $0\frac{3}{4}\frac{3}{8}$ | $0\frac{1}{4}\frac{1}{8}$ | $\frac{3}{8}0\frac{3}{4}$ | $\frac{1}{8}0\frac{1}{4}$ | $\frac{3}{4}\frac{3}{8}0$ | $\frac{1}{4}\frac{1}{8}0$ | $0\frac{1}{4}\frac{5}{8}$ | $0\frac{3}{4}\frac{7}{8}$ | $\frac{5}{8}0\frac{1}{4}$ | $\frac{7}{8}0\frac{3}{4}$ | $\frac{1}{4}\frac{5}{8}0$ | $\frac{3}{4}\frac{7}{8}0$ |
| $e_x^{(k)}$ | 110 | $1\bar{1}0$ | 011 | $01\bar{1}$ | 101 | $\bar{1}01$ | 110 | $1\bar{1}0$ | 011 | $01\bar{1}$ | 101 | $\bar{1}01$ |
| $e_y^{(k)}$ | $\bar{1}10$ | 110 | $0\bar{1}1$ | 011 | $10\bar{1}$ | 101 | $1\bar{1}0$ | $\bar{1}\bar{1}0$ | $01\bar{1}$ | $0\bar{1}\bar{1}$ | $\bar{1}01$ | $\bar{1}0\bar{1}$ |
| $e_z^{(k)}$ | 001 | 001 | 100 | 100 | 010 | 010 | 001 | 001 | 100 | 100 | 010 | 010 |

in Ref. [18]. The magnetoelectric Hamiltonian represents a combination of the product of electric field components $E_\alpha$ and irreducible tensor operators $C_q^k$ coupled with the aid of the coefficients determined by the odd crystal-field parameters. In the second-order approximation,

$$H_{\rm me}^{(2)} = \frac{er_{fd}}{W}\frac{4B_2^3}{7\sqrt{7}}\big(iE_x\big(C_{-1}^2 + C_1^2\big) + E_y\big(C_{-1}^2 - C_1^2\big) + iE_z\big(C_{-2}^2 - C_2^2\big)\big), \quad (1)$$

where $r_{fd} =< f|r|d >$ is the radial integral, $r_{fd} \approx 0.3$–$0.5$ Å, $W \approx 10^5$ cm$^{-1}$ is the distance between the ground $4f^N$ and the exited $4f^{N-1}5^d$ rare-earth ion configurations, $B_2^3$ is the parameter of the odd crystal field responsible for the magnetoelectric Hamiltonian [$V_{\rm odd} = iB_2^3(C_{-2}^3 + C_2^3) + iB_2^5(C_{-2}^5 + C_2^5) + iB_4^5(C_{-4}^5 + C_4^5)$], $B_2^3 \approx 10^3$ cm$^{-1}$ (see Ref. [42]). Magnetoelectric corrections to the spectrum of the rare-earth ion $E_n^{\rm me} =< \psi_n|\widehat{H}_{\rm me}|\psi_n >$ arise due to the entanglement in the exchange field of the states formed by the crystal field. They depend on the type of the rare-earth ion state in a crystal field of the $D_2$ symmetry: singlets ($Pr^{3+}$,$Pm^{3+}$,$Tu^{3+}$) and doublets ($Sm^{3+}$,$Er^{3+}$,$Dy^{3+}$,$Yb^{3+}$). In some cases ($Tb^{3+}$,$Ho^{3+}$), the ground state represents two closely lying singlets, i.e., a quasidoublet, well separated from the overlying energy levels. The magnetic moment of these ions, which is attributed to the splitting of quasidoublet energy levels in the presence of a magnetic field, is oriented collinearly to the definite Ising axis. In the case of the garnet structure, the Ising axis coincides with a particular local axes $e_\alpha^{(k)}$.

### A. Kramers doublet

The splitting of the levels of $n$ Kramers doublet of the $k$th rare-earth ion in a magnetic field reads

$$E_{ni}^{(k)} = E_n + (-1)^i\mu_B\Delta_n(\boldsymbol{H}^{(k)}), i = 1,2;$$
$$\Delta_n(\boldsymbol{H}^{(k)}) = \left[\sum_\alpha \left(g_{n\alpha}H_\alpha^{(k)}\right)^2\right]^{1/2}, \quad (2)$$

where $g_{n\alpha}$ are the components of $g$ tensor of the $n$th doublet, $E_n$ is the energy of $n$th doublet, $H_\alpha^k = \boldsymbol{H}\cdot\boldsymbol{e}_\alpha^{(k)}$, $\boldsymbol{H} = \boldsymbol{H}_{\rm ex} = -\lambda\boldsymbol{M}_{\rm Fe}$ is the $R$-Fe exchange interaction field acting on the rare-earth ions, ($\boldsymbol{H}_{\rm ex} \approx 10$–$20$ T), and $\lambda$ is the molecular field constant. The wave functions $\psi_{ni}^{(k)}$ are determined up to the terms of the first order in $\frac{\mu_B H}{\Delta E}$, where $\Delta E$ is the distance between levels of different doublets (we do not write them here because it is a cumbersome task). The magnetoelectric corrections to the levels $E_{ni}^{(k)}$ [see Eq. (2)] are of the form [18]

$$\delta E_{\rm me}^{ni(k)} = \left\langle\psi_{ni}^{(k)}\middle|\widehat{H}_{\rm me}\middle|\psi_{ni}^{(k)}\right\rangle = (-1)^i\big[c_{n1}E_x^{(k)}H_y^{(k)}\mu_{nz}^{(k)} + c_{n2}E_y^{(k)}H_x^{(k)}\mu_{nz}^{(k)} + c_{n3}E_x^{(k)}H_z^{(k)}\mu_{ny}^{(k)} + c_{n4}E_z^{(k)}H_x^{(k)}\mu_{ny}^{(k)} + c_{n5}E_y^{(k)}H_z^{(k)}\mu_{nx}^{(k)} + c_{n6}E_z^{(k)}H_y^{(k)}\mu_{nx}^{(k)}\big], \quad (3)$$

where $\mu_{n\alpha}^{(k)} = \frac{\mu_B g_{n\alpha}^2}{\Delta_n(\boldsymbol{H}_\alpha^{(k)})}H_\alpha^{(k)}$ is the magnitude of the $\alpha$ component of the magnetic moment of the rare-earth ion state with the energy $E_{n1}^{(k)} = E_n - \mu_B\Delta_n(\boldsymbol{H}^{(k)})$ [see (2)] [$\mu_{n\alpha}^{(k)} = \frac{\partial\Delta_n(\boldsymbol{H}^{(k)})}{\partial H_\alpha^{(k)}}$], $c_{nr} \approx \frac{B_2^3}{W}\frac{er_{fd}}{\Delta E}$, $r = 1,2,\ldots,6$ are the constants depending on the parameters of the magnetoelectric Hamiltonian, the wave functions, and the energy levels of the rare-earth ion in the crystal field. The detailed calculations of $c_{nr}$ are given in Ref. [43]. We average Eq. (3) with the equilibrium density matrix and find the magnetoelectric contribution of the $k$th rare-earth ion in the free energy of a crystal:

$$E_{\rm me}^{(k)} = \frac{\sum_{\rm in}\delta E_{\rm me}^{ni(k)}\exp\left(-E_{ni}^{(k)}/T\right)}{\sum_{\rm in}\exp\left(-E_{ni}^{(k)}/T\right)} > = \mu_B^2\Big[E_x^{(k)}H_y^{(k)}H_z^{(k)}\sum_n\left(c_{n1}g_{nz}^2 + c_{n3}g_{ny}^2\right)F_n^k(T) + E_y^{(k)}H_x^{(k)}H_z^{(k)}\sum_n\left(c_{n2}g_{nz}^2 + c_{n5}g_{nx}^2\right)F_n^k(T) + E_z^{(k)}H_x^{(k)}H_y^{(k)}\sum_n\left(c_{n4}g_{ny}^2 + c_{n6}g_{nx}^2\right)F_n^k(T)\Big], \quad (4)$$

where

$$F_n^k(T) = \frac{\sinh\frac{\mu_B\Delta_n(\boldsymbol{H}^{(k)})}{T}}{\mu_B\Delta_n(\boldsymbol{H}^{(k)})}\frac{\exp\left(\frac{-E_n}{T}\right)}{\sum_m\cosh\frac{\mu_B\Delta_m(\boldsymbol{H}^{(k)})}{T}\exp\left(\frac{-E_m}{T}\right)}. \quad (5)$$

At $\Delta_n(\boldsymbol{H}^{(k)}) < T$, the expressions (4) and (5) are simplified, then

$$E_{\rm me}^{(k)} = d_1E_x^{(k)}h_y^{(k)}h_z^{(k)} + d_2E_y^{(k)}h_x^{(k)}h_z^{(k)} + d_3E_z^{(k)}h_x^{(k)}h_y^{(k)}, \quad (6)$$

where $\boldsymbol{h} = \frac{\boldsymbol{H}}{H}$,

$$d_1(T) = \frac{\mu_B H}{\tau}\sum_n\left(c_{n1}g_{nz}^2 + c_{n3}g_{ny}^2\right)\rho_n(T),$$

$$d_2(T) = \frac{\mu_B H}{\tau}\sum_n\left(c_{n2}g_{nz}^2 + c_{n5}g_{nx}^2\right)\rho_n(T),$$

$$d_3(T) = \frac{\mu_B H}{\tau} \sum_n \left(c_{n4} g_{ny}^2 + c_{n6} g_{nx}^2\right) \rho_n(T),$$

$$\tau = \frac{k_B T}{\mu_B H}, \quad \rho_n(T) = \frac{\exp\left(-E_n/k_B T\right)}{\sum_n \exp\left(-E_n/k_B T\right)}. \tag{7}$$

Since $c_{nr} \approx \frac{B_2^3}{W} \frac{er_{fd}}{\Delta E}$, then $d \approx \frac{1}{\tau} \frac{\mu_B H}{\Delta E} \frac{B_2^3}{W} d_0$, where $d_0 = er_{fd}$ is the dipole moment of an electron. At $B_2^3 \approx 10^3$ cm$^{-1}$, $W \approx 10^5$ cm$^{-1}$, $\frac{\mu_B H}{\Delta E} \approx 10^{-1}$, and $d \approx \frac{d_0}{\tau} 10^{-3}$.

In the case of singlets, $E_{\text{me}}^{(k)}$ is determined by the formula (6), where the constants $d_q (q = 1,2,3)$ are functions weakly dependent on the temperature $T$: $d \approx (\frac{\mu_B H}{\Delta E})^2 \frac{B_2^3}{W} d_0$ (when $T \leqslant \Delta E_{\max}$, $\Delta E_{\max}$ is the width of multiplet in the crystal field) [18].

In the case when the ground state is a quasidoublet reacting to the local component $z$ of the effective magnetic field ($Ho^{3+}$ in $Ho_x Y_{3-x} Fe_5 O_{12}$ [41]), $E_{\text{me}}^{(k)}$ at low temperatures, $T \approx 0$ K, is taken as [18]

$$E_{\text{me}}^{(k)} = -d_1^{\text{Ho}} E_x^{(k)} h_y^{(k)} \gamma_z^{(k)} - d_2^{\text{Ho}} E_y^{(k)} h_x^{(k)} \gamma_z^{(k)}, \tag{8}$$

where $d_1^{\text{Ho}} = c_{01} \mu_z H$, $d_2^{\text{Ho}} = c_{02} \mu_z H$, $\gamma_z^{(k)} = \text{sgn}(\boldsymbol{H} \cdot \boldsymbol{e}_z^{(k)})$, and $\mu_z \approx 10 \mu_B$.

The electric-dipole moment of the rare-earth ions in the $k$th position is determined as

$$P_\alpha^{(k)} = -\frac{\partial E_{\text{me}}^{(k)}}{\partial E_\alpha^{(k)}}, \tag{9}$$

where $E_{\text{me}}^{(k)}$ are defined by Eqs. (6) and (8). The estimated value of the electric-dipole moment of the rare-earth Ising ion [18] is of the order $10^{-2}$ Debye at $T \approx 0$ K in the exchange field $H_{\text{ex}} \approx 10$ T. The structure of the magnetic and electric-dipole moments of $Eu^{3+}$ ions in the primitive cell of europium iron garnet is shown in Fig. 1.

Now, we proceed to the consideration of the electric-dipole moment structure and domain wall polarization in rare-earth iron garnets. We explore separately two cases: (1) the ions with singlet and doublet states at $k_B T \gg \Delta_k$ and (2) the strongly anisotropic Ising ions ($Ho^{3+}$ $Ho_x Y_{3-x} Fe_5 O_{12}$) at low temperatures $k_B T \ll \Delta_k$.

### B. Singlet and doublet ground states at $k_B T > \Delta_k$

As follows from Eqs. (6) and (9), the electric-dipole moments of the considered rare-earth ions are of the form

$$\boldsymbol{P}^{(k)} = d_1 h_y^{(k)} h_z^{(k)} \boldsymbol{e}_x^{(k)} + d_2 h_x^{(k)} h_z^{(k)} \boldsymbol{e}_y^{(k)} + d_3 h_x^{(k)} h_y^{(k)} \boldsymbol{e}_z^{(k)}. \tag{10}$$

The structure of the electric-dipole moments (10) depends on the direction of $\boldsymbol{M}_{\text{Fe}}$, which is determined by the magnetic anisotropy of the rare-earth iron garnets. The magnetic anisotropy of the rare-earth iron garnets is attributed to the presence of the rare-earth ions. At not too high temperatures ($T > 100$ K), the magnetic anisotropy energy acquires the form

$$E_{\text{an}} = -K \left(h_x^4 + h_y^4 + h_z^4\right), \tag{11}$$

where $x, y, z$ are the crystallographic axes. In most cases, $K > 0$ (except $Er_3 Fe_5 O_{12}$, see, e.g., Ref. [41]), hence the "easy axes" coincide with the $\langle 111 \rangle$ crystallographic directions. In a single-domain sample, the homogeneous exchange field $\boldsymbol{h} \| [\bar{1}\bar{1}\bar{1}]$ (at $\boldsymbol{M}_{\text{Fe}} \| [\bar{1}\bar{1}\bar{1}]$) gives rise to the electric-dipole moments:

$$\boldsymbol{P}^{(2,4,6)} = \frac{\sqrt{2}}{3} d_1 \boldsymbol{e}_x^{(2,4,6)}, \quad \boldsymbol{P}^{(1,3,5)} = \frac{\sqrt{2}}{3} d_2 \boldsymbol{e}_y^{(1,3,5)},$$
$$\boldsymbol{P}^{(k+6)} = -\boldsymbol{P}^{(k)}, \quad k = 1,2,\ldots,6, \tag{12}$$

where $d_1, d_2, d_3$ are determined by the formula (7). The distribution of the electric-dipole moments (12) in the primitive cell is described by three-dimensional irreducible representations [44] $\tau_8$ and $\tau_8'$ of the space group $O_h^{10}$ with mixing of the modes $\tau_8'(q'q'q') + \tau_8(qqq)$, $q' = \frac{d_2 + d_1}{6}$ $q = \frac{d_2 - d_1}{6}$.

### C. Magnetoelectricity of domain walls in rare-earth iron garnets

In cubic crystals, four types of domain walls, 71°,90°,109°,180°, can be realized. Our final results do not significantly depend on the particular type of the wall. It is known that the 71° domain walls are energetically favorable in crystals with the $\langle 111 \rangle$ "easy axes" and are typical for the most known rare-earth iron garnets. We explore the magnetoelectric effect in the vicinity of these most stable walls. At first, we consider the Bloch domain wall with the vector $\boldsymbol{M}_{\text{Fe}}$ rotating on a 71° angle from the direction [111] to the direction [11$\bar{1}$] along the $\tilde{z} = [\bar{1}10]$ axis. In this case,

$$\boldsymbol{h} = -\boldsymbol{e}_{\tilde{x}} \cos\phi - \boldsymbol{e}_{\tilde{y}} \sin\phi, \tag{13}$$

where $\phi$ is the azimuthal angle determining the orientation of the vector $\boldsymbol{h} = (\sin\theta\cos\phi, \sin\theta\sin\phi, \cos\theta)$ in the local coordinate frame ($\boldsymbol{e}_{\tilde{x}} = [111]$, $\boldsymbol{e}_{\tilde{y}} = [11\bar{2}]$, $\boldsymbol{e}_{\tilde{z}} = [\bar{1}10]$), $\theta = \pi/2$. The dependence of angle $\phi$ on $\tilde{z}$ coordinate in the 71° Bloch domain wall is given by the formula

$$\phi = \arctan\frac{1}{\sqrt{2}} + \arctan\frac{1}{\sqrt{2}} \tanh\frac{\tilde{z}\sqrt{\frac{K}{A}}}{\sqrt{3}}, \tag{14}$$

where $A$ is the constant of nonuniform exchange interaction, $A = (2\text{–}4) \times 10^{-7}$ erg/cm$^2$, for an iron garnet [45,46], $2\gamma \approx 71°$ is the angle of overall reversal magnetization in a Bloch domain wall, $\sin\gamma = \frac{1}{\sqrt{3}}$.

In our case, the magnetic field $h_{x,y}^{(k)} = h_{x,y}^{(k)}(\phi(\tilde{z}))$ is inhomogeneous. The components of vector $\boldsymbol{h}$ in the local $c$ positions are given in Table II.

Making use of the transformed coordinates $\tilde{z}_k$ (A1) and the $\boldsymbol{h}$ components taken from Table II, we find the electric-dipole moment per unit cell:

$$\Delta \boldsymbol{P} = \sum_{k=1}^{12} \boldsymbol{P}^{(k)} = \eta \sum_{i=1,2,3} d_i \boldsymbol{\Phi}_i, \tag{15}$$

$$\boldsymbol{\Phi}_1 = \frac{\partial\phi}{\partial\zeta}\Big[ -\frac{1}{4}\sqrt{\frac{3}{2}} \cos(\gamma + 2\phi)(314)$$
$$+ \cos(\gamma - 2\phi)(13\bar{4}) + \frac{1}{4}\cos 2(\gamma - \phi)(1\bar{1}0)\Big],$$

TABLE II. The $\boldsymbol{h}$ components in the local $c$ positions.

| | | |
|---|---|---|
| $h_x^{(1,7)} = \cos(\gamma - \phi(\tilde{z}_{1,7}))$ | $h_y^{(1,7)} = 0$ | $h_z^{(1,7)} = \sin(\gamma - \phi(\tilde{z}_{1,7}))$ |
| $h_x^{(2,8)} = 0$ | $h_y^{(2,8)} = \pm\cos(\gamma - \phi(\tilde{z}_{2,8}))$ | $h_z^{(2,8)} = \sin(\gamma - \phi(\tilde{z}_{2,8}))$ |
| $h_x^{(3,9)} = \frac{\sqrt{3}}{2}\sin(2\gamma - \phi(\tilde{z}_{3,9}))$ | $h_y^{(3,9)} = \mp\frac{\sqrt{3}}{2}\sin(\phi(\tilde{z}_{3,9}))$ | $h_z^{(3,9)} = \frac{1}{\sqrt{2}}\cos(\gamma + \phi(\tilde{z}_{3,9}))$ |
| $h_x^{(4,10)} = \frac{\sqrt{3}}{2}\sin(\phi(\tilde{z}_{4,10}))$ | $h_y^{(4,10)} = \pm\frac{\sqrt{3}}{2}\sin(2\gamma - \phi(\tilde{z}_{4,10}))$ | $h_z^{(4,10)} = \frac{1}{\sqrt{2}}\cos(\gamma + \phi(\tilde{z}_{4,10}))$ |
| $h_x^{(5,11)} = \frac{\sqrt{3}}{2}\sin(2\gamma - \phi(\tilde{z}_{5,11}))$ | $h_y^{(5,11)} = \pm\frac{\sqrt{3}}{2}\sin(\phi(\tilde{z}_{5,11}))$ | $h_z^{(5,11)} = \frac{1}{\sqrt{2}}\cos(\gamma + \phi(\tilde{z}_{5,11}))$ |
| $h_x^{(6,12)} = -\frac{\sqrt{3}}{2}\sin(\phi(\tilde{z}_{6,12}))$ | $h_y^{(6,12)} = \pm\frac{\sqrt{3}}{2}\sin(2\gamma - \phi(\tilde{z}_{6,12}))$ | $h_z^{(6,12)} = \frac{1}{\sqrt{2}}\cos(\gamma + \phi(\tilde{z}_{6,12}))$ |

$$\boldsymbol{\Phi}_2 = \frac{\partial\phi}{\partial\zeta}\Big[-\cos 2(\gamma-\phi)(\bar{1}10) - \frac{1}{4}\sqrt{\frac{3}{2}}\cos(\gamma-2\phi)(\bar{3}\bar{1}4) - \cos(\gamma+2\phi)(\bar{1}32)\Big],$$

$$\boldsymbol{\Phi}_3 = \frac{3}{8\sqrt{2}}(\bar{1}10)\sin 2(\phi-\gamma)\frac{\partial\phi}{\partial\zeta}, \tag{16}$$

where $\eta = \frac{a}{l_0}$, $\zeta = \frac{\tilde{z}}{l_0}$, $l_0 = \sqrt{\frac{2A}{K}} \approx 100$ Å is the characteristic width of the domain wall, $(pqt) = p[100] + q[010] + t[001]$ is a vector, and $\phi(\zeta)$ is determined by Eq. (14).

Figure 2 shows the dependencies of $\boldsymbol{\Phi}_i$ $(i = 1,2,3)$ components on the coordinate $\zeta = \frac{\tilde{z}}{l_0}$ in the 71° domain wall. The resulting polarization depends on the relation between $d_1$, $d_2$, and $d_3$ coefficients that should be determined in each particular case. The polarization of the domain wall is defined by the formula $\boldsymbol{P}(\tilde{z}) = \frac{\Delta\boldsymbol{P}}{\Delta V}$, where $\Delta V$ is the volume of the primitive cell.

### D. Magnetoelectricity of strongly anisotropic rare-earth Ising ions. Polarization of the domain walls of holmium-yttrium iron garnets

In this section, we consider the strongly anisotropic Ising ions taking as an example $Ho^{3+}$ ions in iron garnet [18] $Ho_xY_{3-x}Fe_5O_{12}$ $0 \leqslant x \leqslant 3$. The ground state of holmium ion is quasidoublet, well separated from the excited energy levels. The magnetic moment of the $Ho^{3+}$ ion is due to the splitting of the quasidoublet ground-energy levels in an effective magnetic field and can be oriented either along or versus the local axis (since the splitting is $\Delta_k = \pm\mu_z H_z^{(k)}$). At low temperatures, the energy of the magnetic anisotropy per one rare-earth ion reads

$$E_{\text{an}} = -K\tau\left(\ln\cosh\frac{h_x}{\tau} + \ln\cosh\frac{h_y}{\tau} + \ln\cosh\frac{h_z}{\tau}\right), \tag{17}$$

where $K = \frac{x\mu_z H}{3}$ is the constant of the magnetic anisotropy per one rare-earth ion, $\mu_z$ is the average value of the operator of Ising doublet magnetic moment, $x$ is the concentration of $Ho^{3+}$ ions, and $\tau = \frac{k_B T}{\mu_z H}$. Note that at $\tau \ll 1$, formula (17) acquires the form

$$E_{\text{an}} = -K(|h_x| + |h_y| + |h_z|), \tag{18}$$

where $K$ is the constant of the magnetic anisotropy per unit volume, at low temperatures [41] $K \approx 10^7$ erg/cm$^3$ in $Ho_3Fe_5O_{12}$. The expression (18) is quite different from its classical form (11) as was indicated in Ref. [41].

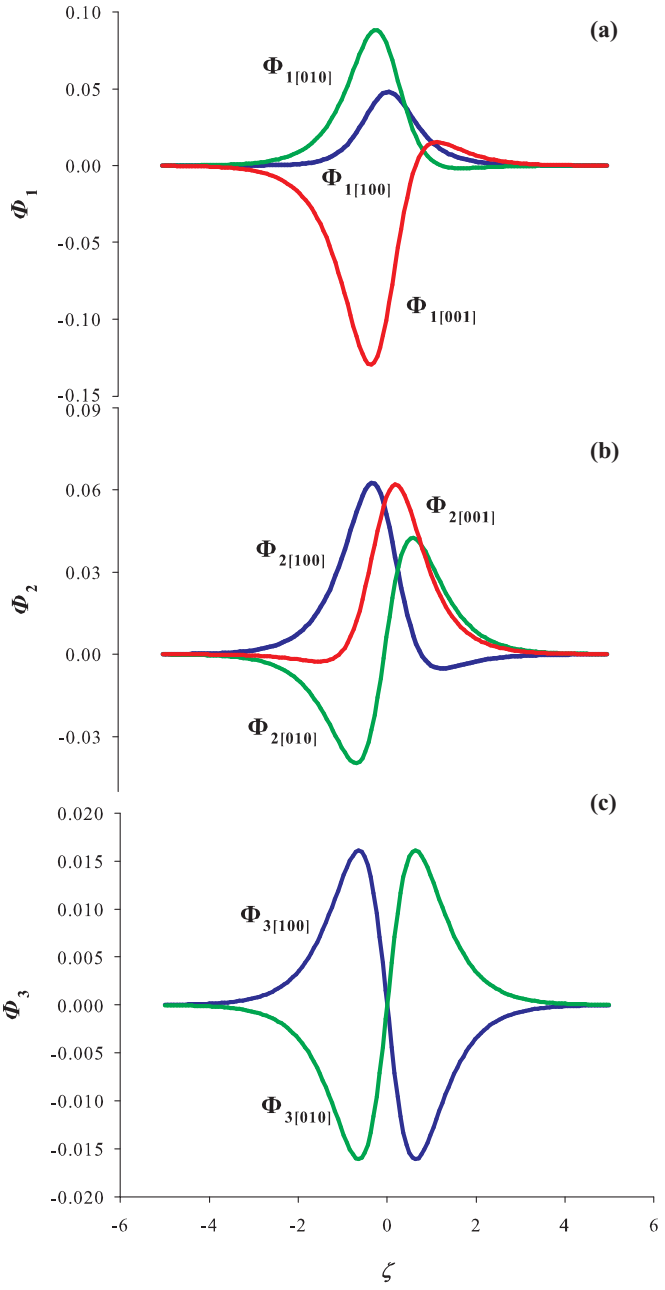


FIG. 2. (Color online) The dependence of the $\Phi_1(\zeta), \Phi_2(\zeta)$, and $\Phi_3(\zeta)$ components on the coordinate $\zeta$ in the 71° Bloch domain wall related to the rare-earth ions; the blue line corresponds to the projection $\boldsymbol{\Phi}_{[100]}$, the green line corresponds to the projection $\boldsymbol{\Phi}_{[010]}$, and the red line corresponds to the projection $\boldsymbol{\Phi}_{[001]}$.

The structure of the 71° Bloch domain wall where $\boldsymbol{M}_{\mathrm{Fe}}$ rotates from the [111] axis to the [11$\bar{1}$] axis over $\tilde{z} = [\bar{1}10]$ axis is calculated analytically (see Appendix B). Note that analytical solutions can be found only in the limiting cases of low and high temperatures.

From Eqs. (8) and (9), we find the expression for the electric-dipole moment of the $k$th ion:

$$\boldsymbol{P}^{(k)} = -\gamma_z^{(k)}\left(d_1^{\mathrm{Ho}} h_y^{(k)} \boldsymbol{e}_x^{(k)} + d_2^{\mathrm{Ho}} h_x^{(k)} \boldsymbol{e}_y^{(k)}\right). \tag{19}$$

The structure of the electric-dipole moments of $Ho^{3+}$ ion in the homogeneous exchange field $\boldsymbol{h}||[\bar{1}\bar{1}\bar{1}]$ in general is similar to the structure shown in Fig. 1. It is determined by the three-dimensional irreducible representations [44] $\tau_8$ and $\tau_8'$ of the space group $O_h^{10}$.

The electric-dipole moments of the domain walls in HoIG read

$$\boldsymbol{P}^{(k)} = \pm\left(d_1^{\mathrm{Ho}} h_y^{(k)} \boldsymbol{e}_x^{(k)} + d_2^{\mathrm{Ho}} h_x^{(k)} \boldsymbol{e}_y^{(k)}\right); \tag{20}$$

here the positive sign corresponds to the case $\tilde{z} > 0 (\phi > \gamma)$, $k = 1,2,7,8$ and the negative sign corresponds to the case $\tilde{z} < 0 (\phi < \gamma)$, $k \neq 1,2,7,8$. To write Eq. (20) we take into account the fact that the magnetization of the rare-earth ion located in 1, 2 and 3, 8 positions (see the Table I) is flipped in the center of the domain wall. At $\tilde{z} < 0 (\phi < \gamma)$, all $\gamma_z^{(k)} = \gamma$ and at $\tilde{z} > 0 (\phi > \gamma)$, $\gamma_z^{(1)} = \gamma_z^{(2)} = \gamma_z^{(7)} = \gamma_z^{(8)} = \gamma, \gamma_z^{(k)} = \gamma$ for the remaining $k$.

The resulting electric-dipole moment of the primitive cell is

$$\Delta \boldsymbol{P} = \eta \sum_{i=1,2} d_i \boldsymbol{\Phi}_i, \tag{21}$$

where

$$\boldsymbol{\Phi}_1 = \frac{\partial \phi}{\partial \zeta}\Big[ -\frac{\sqrt{3}}{4}\cos\phi(314) - \frac{\sqrt{3}}{4}\cos(2\gamma - \phi)(13\bar{4}) \mp \cos(\alpha + \phi)(1\bar{1}0)\Big],$$

$$\boldsymbol{\Phi}_2 = \frac{\partial \phi}{\partial \zeta}\Big[ \frac{\sqrt{3}}{4}\cos\phi(134) + \frac{\sqrt{3}}{4}\cos(2\gamma - \phi)(31\bar{4}) \pm \cos(\alpha + \phi)(\bar{1}01)\Big]. \tag{22}$$

The upper sign in Eq. (22) corresponds to the case $\tilde{z} < 0$, the lower sign corresponds to the case $\tilde{z} > 0$, the notation for vectors $(pqt)$ is taken the same as in formula (15).

Figure 3 shows the dependencies of projections $\boldsymbol{\Phi}_{[100]}$, $\boldsymbol{\Phi}_{[010]}$, and $\boldsymbol{\Phi}_{[010]}$ of vectors $\boldsymbol{\Phi}_1$, $\boldsymbol{\Phi}_2$, and $\boldsymbol{\Phi} = \boldsymbol{\Phi}_1 + \boldsymbol{\Phi}_2$ on the coordinate $\zeta$ at equal values $d_1^{\mathrm{Ho}} = d_2^{\mathrm{Ho}} = d^{\mathrm{Ho}}$. In this case, polarization vanishes in the center of the domain wall [see Fig. 3(c)].

### E. Magnetoelectricity of $Eu_3Fe_5O_{12}$

Europium iron garnets stand out among the other iron garnets due to their physical properties. EuIG has a relatively small magnetization weakly dependent on the temperature in the low-temperature range ($T \leqslant 300$ K). The magnetic anisotropy of EuIG is mainly attributed to $Eu^{3+}$ ions, it weakly

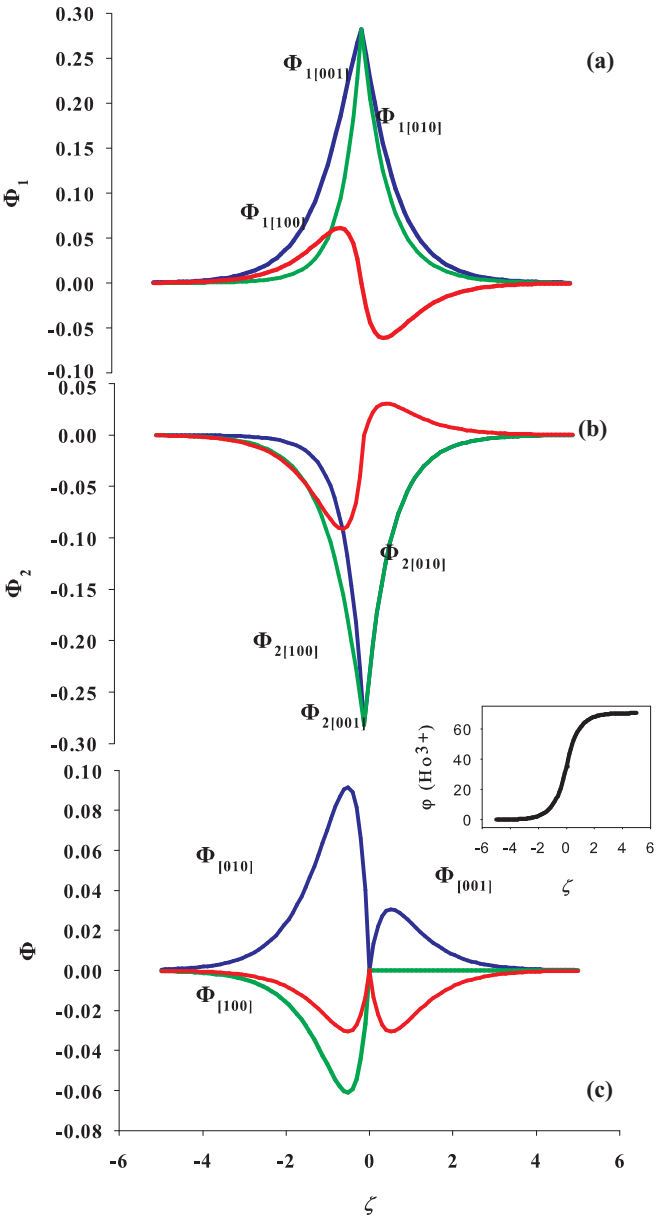


FIG. 3. (Color online) The dependence of the $\Phi_1(\zeta)$, $\Phi_2(\zeta)$, and $\Phi(\zeta) = \Phi_1(\zeta) + \Phi_2(\zeta)$ components on the coordinate $\zeta$ in the 71° Bloch domain wall related to $Ho^{3+}$ ions ($d_1^{\mathrm{Ho}} = d_2^{\mathrm{Ho}}$); the blue line corresponds to the projection $\boldsymbol{\Phi}_{[100]}$, the green line corresponds to the projection $\boldsymbol{\Phi}_{[010]}$, and the red line corresponds to the projection $\boldsymbol{\Phi}_{[001]}$. The insert shows the dependence $\phi = \phi(\zeta)$ illustrating the profile of the 71° Bloch domain wall.

decreases when the temperature is enhanced. These differences are owed to the ground state of $Eu^{3+}$ ion, which is the singlet with $J = 0$, and as a consequence, the magnetic properties of this ion are entirely determined by the mixing in the magnetic field of the singlet state $J = 0$ with the excited states (the triplet $J = 1$ separated by an energy gap $\Delta_1 \approx 350$ cm$^{-1}$ from the lower lying ground level and the multiplet $J = 2$ located at the distance $\Delta_2 = 3\,\Delta_1 \approx 1050$ cm$^{-1}$ from the ground state). The magnetic field $\boldsymbol{H} = -\lambda \boldsymbol{M}_{\mathrm{Fe}}$ whose magnitude is determined by the relation $\mu_B H = 15$ cm$^{-1}$ acts on $Eu^{3+}$ ions in EuIG. The interaction of a $Eu^{3+}$ ion with the exchange field

in the case when the exchange anisotropy is neglected is of the form $V_z = 2\mu_B \boldsymbol{S}\boldsymbol{H}$.

We neglect the influence of the crystal field on the states of a $Eu^{3+}$ ion and find the wave function of the ground state up to the second-order terms in $\boldsymbol{H}$:

$$\begin{aligned}\psi_s = |00\rangle &\left[1 - 8\left(\frac{\mu_B H}{\Delta_i}\right)^2\right] \\ &+ \frac{4\mu_B H}{\Delta_i} \sum_{\nu=0,\pm1} (-1)^\nu h_\nu |1-\nu\rangle \\ &+ \frac{12(\mu_B H)^2}{\Delta_1 \Delta_2}\left[\sqrt{3}\left(h_z^2 - \frac{1}{3}\right)|20\rangle\right. \\ &- 2h_z(h_{-1}|21\rangle + h_{+1}|2-1\rangle) \\ &\left.\sqrt{2}\left(h_{-1}^2|22\rangle + h_{+1}^2|2-2\rangle\right)\right], \end{aligned} \tag{23}$$

where $\boldsymbol{h} = \frac{\boldsymbol{H}}{H}$, $h_0 = h_z$, and $h_{\pm1} = \mp\frac{1}{\sqrt{(2)}}(h_x \pm i h_y)$. The magnetoelectricity of the $Eu^{3+}$ ions is determined by Hamiltonian (1). Averaging (1) with the wave functions (23), we find

$$E_{\rm me}^{(k)} = -d\left(E_x^{(k)} h_y^{(k)} h_z^{(k)} + E_y^{(k)} h_x^{(k)} h_z^{(k)} + E_z^{(k)} h_x^{(k)} h_y^{(k)}\right), \tag{24}$$

$$d = \frac{e r_{fd}}{W} B_2^3 \left(\frac{\mu_b H}{\Delta_1}\right)^2 \frac{128}{7\sqrt{7}}\left(\frac{1}{3}\sqrt{\frac{2}{5}} + \frac{1}{5}\sqrt{\frac{3}{2}}\right). \tag{25}$$

In this case, the magnetoelectric energy $E_{\rm me}$ is defined by the single constant $d$ in contrast to the general case (7). The electric-dipole moments of $Eu^{3+}$ are determined by the formula (10) with $d_1 = d_2 = d_3 = d$, where $d$ is defined by Eq. (25). The constant of magnetic anisotropy $K = 10^5\,{\rm erg/cm^3}$ for $Eu_3Fe_5O_{12}$ is taken from Refs. [41,46] and the "easy axes" in this case correspond to the crystallographic directions $\langle 111\rangle$.

The structure of the magnetic and the electric dipole moments of $Eu^{3+}$ ions induced by the homogeneous exchange field $\boldsymbol{h}||[\bar{1}\bar{1}\bar{1}]$ in the primitive cell is shown in Fig. 1. It is described by the three-dimensional irreducible representation [44] $\tau_8'$ with a mode entanglement $\tau_8'(qqq)$, where $q = -\frac{d}{3}$. The electric-dipole moments of $Eu^{3+}$ ions in the (111) oriented plane in the primitive cell are shown in Fig. 4.

At $d_1 = d_2 = d_3 = d$ (25), the polarization of the 71° Bloch domain wall of EuIG determined by formula (15) reads

$$\Delta \boldsymbol{P} = \eta d(\boldsymbol{\Phi}_1 + \boldsymbol{\Phi}_2 + \boldsymbol{\Phi}_3). \tag{26}$$

Figure 5 shows the dependencies of vector $\boldsymbol{\Phi} = \frac{\Delta \boldsymbol{P}}{d}$ on $\zeta$ coordinate in the vicinity of a Bloch domain wall in EuIG. The dependence $\phi = \phi(\zeta)$ in the 71° Bloch domain wall is given in the insert of Fig. 5. It should be noted that besides $Eu^{3+}$ the singlet ground state is realized in $Tm^{3+}$,$Pr^{3+}$, and $Pm^{3+}$.

Thus we have considered the magnetoelectricity of the 71° Bloch domain walls, which are typical for the majority of single crystals. In the iron garnet films, the 180° Bloch domain walls appear to be energetically more preferable. In the case of the 180° Bloch domain walls, all the presented results remain valid [for the (111) oriented iron garnet films]. The magnetoelectricity of the 180° Neel domain walls has been also considered (see Appendix C).

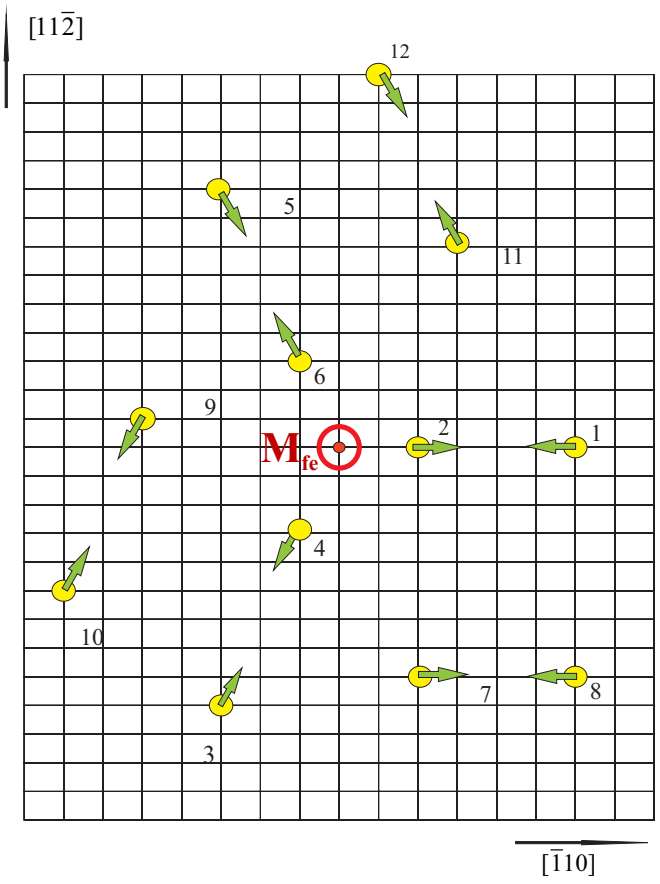


FIG. 4. (Color online) The structure of electric-dipole moments of $Eu^{3+}$ ions in the primitive cell of EuIG at $\boldsymbol{M}_{\rm Fe}||[111]$ as a projection on the (111)-oriented plane.

## IV. CONCLUSION

Our findings show that electric polarization arises in the vicinity of magnetic domain walls independently of their type

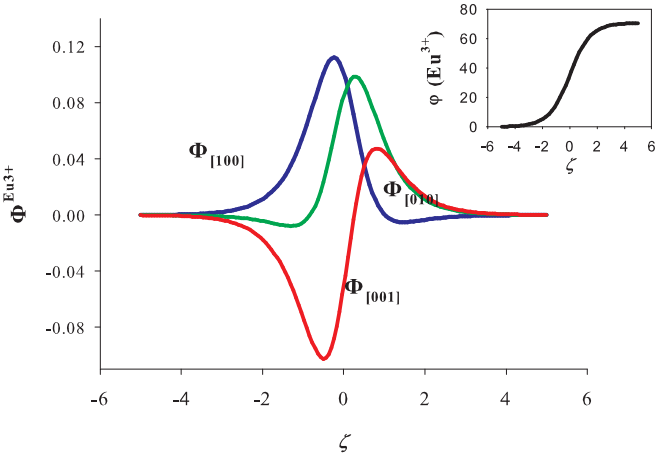


FIG. 5. (Color online) The dependence of vector $\boldsymbol{\Phi}^{Eu^{3+}}(\zeta)$ components on the coordinate $\zeta$ in the 71° Bloch domain wall related to $Eu^{+3}$ ions; the blue line corresponds to $\boldsymbol{\Phi}_{[100]}$, the green line corresponds to $\boldsymbol{\Phi}_{[010]}$, and the red line corresponds to $\boldsymbol{\Phi}_{[001]}$. The insert shows the dependence $\phi = \phi(\zeta)$ illustrating the profile of the 71° Bloch domain wall.

(Bloch, Neel, etc.) due to inhomogeneous magnetoelectric interaction. The character of the polarization distribution depends on the ground state of the rare-earth ion. The experiments carried out on iron garnets [14,15,17,35] show that the electric field induces domain wall dynamics and that the properties of the domain wall polarization depend on the configuration of the applied electric field.

In this paper, we discussed a new mechanism for the magnetoelectric effect in rare-earth iron garnets. The rare-earth ions acquire electric-dipole moments due to the action of a crystal field of a lowered symmetry. The effective magnetic field created by the iron sublattice orders magnetic and electric-dipole moments of the rare-earth ions and leads to the formation of an antiferroelectric structure. In the presence of magnetic domain walls, the effective magnetic field becomes inhomogeneous, and as a consequence the antiferroelectric structure rearranges and nonzero polarization appears.

A salient feature of the studied effects is that both Bloch and Neel domain walls are the sources of inhomogeneous magnetic field inducing electric polarization. In accordance with conventional concepts of the inhomogeneous magnetoelectric effect [13,38], the electric polarization can not arise when the vectors of spin modulation and normal to the spin rotation plane are collinear, which is the case of magnetic helicoids and Bloch domain walls. We demonstrate that the electric polarization can be generated by the rare-earth subsystem even for the Bloch domain structure of the iron sublattice due to the presence of an antiferroelectric structure.

A magnetic domain wall is a chiral object characterized by the direction of the spin rotation across the wall (left or right screw) [47], hence the direction of the polar moment in the domain wall depends on its chirality. The chirality can be switched by a magnetic or an electric field, which in turn leads to the switching of the polarization. The coercitivity of such a dipole moment can be sufficiently small ($\approx 10^{-4}$ T), which is of interest for nanoelectronics.

## ACKNOWLEDGMENTS

This work was supported by the Russian Foundation for Basic Research (Grant No. 14-02-91374 ST-a), the Russian Ministry of Education and Science (Project No. 2528), and 50 Labs Initiative of Moscow Institute of Physics and Technology, MFTI.

## APPENDIX A: THE RARE-EARTH ION COORDINATES AND EFFECTIVE MAGNETIC FIELD COMPONENTS *h* IN *c* POSITIONS IN THE LOCAL REFERENCE FRAME ($e_x$ = [111], $e_y$ = [11$\bar{2}$], $e_z$ = [$\bar{1}$10])

The coordinates $\tilde{z}_k$ for all 12 ion positions in the unit cell expressed in the units of the cell edge length are determined as follows:

$$\tilde{z}_1 = a\frac{3}{4\sqrt{2}}, \quad \tilde{z}_2 = a\frac{1}{4\sqrt{2}},$$
$$\tilde{z}_3 = -a\frac{3}{8\sqrt{2}}, \quad \tilde{z}_4 = -a\frac{1}{8\sqrt{2}},$$
$$\tilde{z}_5 = -a\frac{3}{8\sqrt{2}}, \quad \tilde{z}_6 = -a\frac{1}{8\sqrt{2}},$$
$$\tilde{z}_7 = a\frac{1}{4\sqrt{2}}, \quad \tilde{z}_8 = a\frac{3}{4\sqrt{2}},$$
$$\tilde{z}_9 = -a\frac{5}{8\sqrt{2}}, \quad \tilde{z}_{10} = -a\frac{7}{8\sqrt{2}},$$
$$\tilde{z}_{11} = a\frac{3}{8\sqrt{2}}, \quad \tilde{z}_{12} = a\frac{1}{8\sqrt{2}}. \tag{A1}$$

## APPENDIX B: THE 71° BLOCH DOMAIN WALL STRUCTURE FOR THE ISING RARE-EARTH IONS

The total energy of the Ising rare-earth ions in the effective magnetic field of the iron subsystem in the low-temperature case is written as follows:

$$E = \int \left( A\left(\frac{\partial\phi}{\partial\tilde{z}}\right)^2 + K(|h_x| + |h_y| + |h_z|)\right)d\tilde{z}. \tag{B1}$$

The variational problem for (B1) acquires the following form:

$$E = \delta\int_{-\infty}^{+\infty}\left[A\left(\frac{\partial\phi}{\partial\tilde{z}}\right)^2 - K\sqrt{2}(\sin(\alpha+\phi) + |\cos(\alpha+\phi)|)\right]d\tilde{z}, \tag{B2}$$

$$\phi(-\infty) = 0, \quad \phi(+\infty) = 2\gamma \approx 71^\circ, \quad \frac{d\phi}{d\tilde{z}}(\pm\infty) = 0. \tag{B3}$$

The Euler-Lagrange equations for (B2) and (B3) are represented as

$$-A\left(\frac{\partial\phi}{\partial\tilde{z}}\right)^2 - (\sin(\alpha+\phi) + |\cos(\alpha+\phi)|) = -\sqrt{3}K. \tag{B4}$$

We find a solution of Eq. (B4) for two cases (by taking into account the modulus $|\cos(\alpha+\phi)|$):

1. $0 \leqslant \phi \leqslant \gamma, \tilde{z} \leqslant 0$

$$\tan\frac{\phi}{4} = \tan\frac{\gamma}{4}\exp\left(3^{1/4}\sqrt{\frac{K}{2A}}\tilde{z}\right),$$
$$\frac{\partial\phi}{\partial\tilde{z}} = 3^{1/4}\sqrt{\frac{K}{2A}(1-\cos\phi)}; \tag{B5}$$

2. $\gamma \leqslant \phi \leqslant 2\gamma, \tilde{z} > 0$

$$\tan\left(\frac{\gamma}{2} - \frac{\phi}{4}\right) = \tan\frac{\gamma}{4}\exp\left(-3^{1/4}\sqrt{\frac{K}{2A}}\tilde{z}\right),$$
$$\frac{\partial\phi}{\partial\tilde{z}} = 3^{1/4}\sqrt{\frac{K}{2A}(1-\cos(2\gamma-\phi))}. \tag{B6}$$

Since $\gamma/4 \approx 8.87^\circ$, $\tan\gamma/4 = 0.15 \ll 1$, the solution $\phi(\tilde{z})$ in (B5) and (B6) can be represented as

$$\phi = \gamma\exp\left(3^{1/4}\sqrt{\frac{K}{2A}}\tilde{z}\right), \ \tilde{z} \leqslant 0,$$
$$\phi = \gamma\left[2 - \exp\left(-3^{1/4}\sqrt{\frac{K}{2A}}\tilde{z}\right)\right], \ \tilde{z} > 0. \tag{B7}$$

## APPENDIX C: NEEL DOMAIN WALL STRUCTURE

We consider the Neel domain wall where the magnetization vector $\boldsymbol{M}_{\mathrm{Fe}}$ rotates in the $(\bar{1}10)$ plane from the $[\bar{1}\bar{1}\bar{1}]$ axis to the $[111]$ axis ($\boldsymbol{e}_x = [111], \boldsymbol{e}_y = [11\bar{2}], \boldsymbol{e}_z = [\bar{1}10]$). The exchange field acting on the rare-earth ion is written as

$$\boldsymbol{h} = -\boldsymbol{e}_{\tilde{x}} \cos\phi - \boldsymbol{e}_{\tilde{y}} \sin\phi. \tag{C1}$$

The magnetization rotates in the $\tilde{X}O\tilde{Z}$ plane, hence $\phi(\pm\infty) = \pm\frac{\pi}{2}$. In a general case, (singlet, doublet at $\Delta \ll kT, \chi_k \approx \frac{1}{T}$),

$$\boldsymbol{P}^{(k)} = d_1 h_y^{(k)} h_z^{(k)} \boldsymbol{e}_x^{(k)} + d_2 h_x^{(k)} h_z^{(k)} \boldsymbol{e}_y^{(k)} + d_3 h_x^{(k)} h_y^{(k)} \boldsymbol{e}_z^{(k)}. \tag{C2}$$

The components $h_\alpha^{(k)}$ are determined as

$$\begin{aligned}
h_z^{(1,2,7,8)} &= -\frac{1}{\sqrt{3}}\sin\phi, \quad h_z^{(3,4,9,10)} = -\sqrt{\frac{5}{6}}\sin(\phi+\delta),\\
h_z^{(5,6,11,12)} &= \sqrt{\frac{5}{6}}\sin(\delta-\phi), \quad h_y^{(1,7)} = \pm\cos\phi,\\
h_y^{(2,8)} &= \mp\sqrt{\frac{2}{3}}\sin\phi, \quad h_y^{(3,5,9,11)} = \mp\frac{1}{2}\cos\phi,\\
h_y^{(4,10)} &= \pm\sqrt{\frac{11}{12}}\sin(\beta-\phi),\\
h_y^{(6,12)} &= \mp\sqrt{\frac{11}{12}}\sin(\beta+\phi),
\end{aligned} \tag{C3}$$

where

$$\begin{aligned}
\sin\delta &= \sqrt{\frac{3}{5}}, \quad \cos\delta = \sqrt{\frac{2}{5}},\\
\sin\beta &= \sqrt{\frac{3}{11}}, \quad \cos\beta = \sqrt{\frac{8}{11}}.
\end{aligned} \tag{C4}$$

TABLE III. Products of $\boldsymbol{h}$ components.

| k | $h_y^{(k)}h_z^{(k)}$ | $h_x^{(k)}h_z^{(k)}$ | $h_x^{(k)}h_y^{(k)}$ |
|---|---|---|---|
| 1, 7 | $\mp\frac{1}{2\sqrt{3}}\sin 2\phi$ | $\frac{\sqrt{2}}{3}\sin^2\phi$ | $\mp\frac{1}{2}\sqrt{\frac{2}{3}}\sin 2\phi$ |
| 2, 8 | $\pm\frac{\sqrt{2}}{3}\sin^2\phi$ | $\frac{1}{2\sqrt{3}}\sin 2\phi$ | $\pm\frac{1}{2}\sqrt{\frac{2}{3}}\sin 2\phi$ |
| 3, 9 | $\pm\frac{1}{2}\sqrt{\frac{5}{6}}f_1(\phi)$ | $-\sqrt{\frac{55}{72}}f_2(\phi)$ | $\mp\frac{1}{2}\sqrt{\frac{11}{12}}f_3(-\phi)$ |
| 4, 10 | $\mp\sqrt{\frac{55}{72}}f_2(\phi)$ | $-\frac{1}{2}\sqrt{\frac{5}{6}}f_1(\phi)$ | $\pm\frac{1}{2}\sqrt{\frac{11}{12}}f_3(-\phi)$ |
| 5, 11 | $\mp\frac{1}{2}\sqrt{\frac{5}{6}}f_1(-\phi)$ | $-\sqrt{\frac{55}{72}}f_2(-\phi)$ | $\pm\frac{1}{2}\sqrt{\frac{11}{12}}f_3(\phi)$ |
| 6,12 | $\mp\sqrt{\frac{55}{72}}f_2(-\phi)$ | $\frac{1}{2}\sqrt{\frac{5}{6}}f_1(-\phi)$ | $\mp\frac{1}{2}\sqrt{\frac{11}{12}}f_3(\phi)$ |

The products of the $h$ components are given in Table III. We use formula (C2), and Tables I and III, to find the electric-dipole moment for the Neel domain wall:

$$\begin{aligned}
\Delta\boldsymbol{P} = \eta\frac{\partial\phi}{\partial\zeta}\Bigg\{ & d_1\Bigg[-\frac{1}{2\sqrt{2}}\left(\frac{\cos 2\phi}{\sqrt{3}}\boldsymbol{e}_x^{(1)} + \frac{\sqrt{2}}{3}\sin 2\phi\,\boldsymbol{e}_x^{(2)}\right)\\
&+\frac{1}{16}\sqrt{\frac{5}{3}}\cos(\delta+2\phi)\left(\boldsymbol{e}_x^{(3)} - 3\boldsymbol{e}_x^{(5)}\right)\\
&+\frac{\sqrt{5\cdot 11}}{2\cdot 4\cdot 6}\sin(2\phi+\delta-\beta)\left(3\boldsymbol{e}_x^{(4)} + \boldsymbol{e}_x^{(6)}\right)\Bigg]\\
&+d_2\Bigg[\frac{\sin 2\phi}{6}\boldsymbol{e}_y^{(1)} - \frac{\cos 2\phi}{2\sqrt{6}}\boldsymbol{e}_y^{(2)}\\
&+\frac{\sqrt{5\cdot 11}}{2\cdot 4\cdot 6}\sin(2\phi+\delta-\beta)\left(\boldsymbol{e}_y^{(3)} + 3\boldsymbol{e}_y^{(5)}\right)\\
&-\frac{1}{16}\sqrt{\frac{5}{3}}\cos(\delta+2\phi)\left(3\boldsymbol{e}_y^{(4)} - \boldsymbol{e}_y^{(6)}\right)\Bigg]\\
&+d_3\left[\frac{\cos 2\phi}{\sqrt{3}}(001) - \frac{1}{8}\sqrt{\frac{11}{6}}\cos(\beta+2\phi)(110)\right]\Bigg\}.
\end{aligned} \tag{C5}$$


[1] J. Seidel, L. W. Martin, Q. He, Q. Zhan, Y.-H. Chu, A. Rother, M. Hawkridge, P. Maksymovych, P. Yu, M. Gajek *et al.*, Nat. Mater. **8**, 229 (2009).

[2] D. Meier, J. Seidel, A. Cano, K. Delaney, Y. Kumagai, M. Mostovoy, N. A. Spaldin, R. Ramesh, and M. Fiebig, Nat. Mater. **11**, 284 (2012).

[3] R. Vasudevan, A. Morozovska, E. Eliseev, J. Britson, J.-C. Yang, Y.-H. Chu, P. Maksymovych, L. Chen, V. Nagarajan, and S. Kalinin, Nano Lett. **12**, 5524 (2012).

[4] X.-K. Wei, A. K. Tagantsev, A. Kvasov, K. Roleder, C.-L. Jia, and N. Setter, Nat. Commun. **5** (2014).

[5] J. Yang, C. Yeh, Y. Chen, S. Liao, R. Huang, H. Liu, C. Hung, S. Chen, S. Wu, C. Lai *et al.*, Nanoscale **6**, 10524 (2014).

[6] A. Bhatnagar, A. R. Chaudhuri, Y. H. Kim, D. Hesse, and M. Alexe, Nat. Commun. **4**, 2835 (2013).

[7] Z. Yang, M. Lange, A. Volodin, R. Szymczak, and V. V. Moshchalkov, Nat. Mater. **3**, 793 (2004).

[8] M. Daraktchiev, G. Catalan, and J. F. Scott, Phys. Rev. B **81**, 224118 (2010).

[9] L. W. Martin, Y.-H. Chu, M. B. Holcomb, M. Huijben, P. Yu, S.-J. Han, D. Lee, S. X. Wang, and R. Ramesh, Nano Lett. **8**, 2050 (2008).

[10] Q. He, C.-H. Yeh, J.-C. Yang, G. Singh-Bhalla, C.-W. Liang, P.-W. Chiu, G. Catalan, L. Martin, Y.-H. Chu, J. Scott *et al.*, Phys. Rev. Lett. **108**, 067203 (2012).

[11] Z. Gareeva, O. Diéguez, J. Íñiguez, and A. K. Zvezdin, Phys. Rev. B **91**, 060404 (2015).

[12] A. Zvezdin and A. Pyatakov, Physics-Uspekhi **47**, 416 (2004).

[13] M. Mostovoy, Phys. Rev. Lett. **96**, 067601 (2006).

[14] A. S. Logginov, G. Meshkov, A. Nikolaev, and A. P. Pyatakov, JETP Lett. **86**, 115 (2007).

[15] A. Logginov, G. Meshkov, A. Nikolaev, E. Nikolaeva, A. Pyatakov, and A. Zvezdin, Appl. Phys. Lett. **93**, 182510 (2008).
[16] A. K. Zvezdin and A. P. Pyatakov, Physics-Uspekhi **52**, 845 (2009).
[17] A. Pyatakov, D. Sechin, A. Sergeev, A. Nikolaev, E. Nikolaeva, A. Logginov, and A. Zvezdin, Europhys, Lett. **93**, 17001 (2011).
[18] A. I. Popov, D. I. Plokhov, and A. K. Zvezdin, Phys. Rev. B **90**, 214427 (2014).
[19] G. Catalan, J. Seidel, R. Ramesh, and J. F. Scott, Rev. Mod. Phys. **84**, 119 (2012).
[20] Y. Tokunaga, N. Furukawa, H. Sakai, Y. Taguchi, T.-h. Arima, and Y. Tokura, Nat. Mater. **8**, 558 (2009).
[21] Y. Tokunaga, Y. Taguchi, T.-h. Arima, and Y. Tokura, Nat. Phys. **8**, 838 (2012).
[22] A. K. Zvezdin and A. A. Mukhin, JETP Lett. **88**, 505 (2008).
[23] T. O'Dell, Phil. Mag. **16**, 487 (1967).
[24] M. J. Cardwell, Physica status solidi (b) **45**, 597 (1971).
[25] G. Velleaud, B. Sangare, M. Mercier, and G. Aubert, Solid State Commun. **52**, 71 (1984).
[26] S. Hirakata, M. Tanaka, K. Kohn, E. Kita, K. Siratori, S. Kimura, and A. Tasaki, J. Phys. Soc. Jpn. **60**, 294 (1991).
[27] H. Ogawa, E. Kita, Y. Mochida, K. Kohn, S. Kimura, A. Tasaki, and K. Siratori, J. Phys. Soc. Jpn. **56**, 452 (1987).
[28] S. Takano, E. Kita, K. Siratori, K. Kohn, S. Kimura, and A. Tasaki, J. Phys. Soc. Jpn. **58**, 1145 (1989).
[29] E. Kita, S. Takano, K. Kohn, K. Siratori, S. Kimura, and A. Tasaki, J. Mag. Mag. Mater. **104**, 449 (1992).
[30] R. Pisarev, B. Krichevtsov, V. Gridnev, V. Klin, D. Frohlich, and C. Pahlke-Lerch, J. Phys.: Condens. Matter **5**, 8621 (1993).
[31] S. Takano, E. Kita, K. Siratori, K. Kohn, S. Kimura, and A. Tasaki, Ferroelectrics **161**, 73 (1994).
[32] V. V. Pavlov, R. V. Pisarev, A. Kirilyuk, and T. Rasing, Phys. Rev. Lett. **78**, 2004 (1997).
[33] V. E. Koronovskyy, S. M. Ryabchenko, and V. F. Kovalenko, Phys. Rev. B **71**, 172402 (2005).
[34] Y. Kohara, Y. Yamasaki, Y. Onose, and Y. Tokura, Phys. Rev. B **82**, 104419 (2010).
[35] A. Pyatakov, A. Sergeev, F. Mikailzade, and A. Zvezdin, J. Mag. Mag. Mater. **383**, 255 (2015).
[36] A. Pyatakov, G. Meshkov, and A. Zvezdin, J. Mag. Mag. Mater. **324**, 3551 (2012).
[37] Z. Gareeva, R. Doroshenko, F. Mazhitova, and N. Shulga, J. Mag. Mag. Mater. **385**, 60 (2015).
[38] V. G. Bar'yakhtar, V. A. L'vov, and D. A. Yablonskii, JETP Lett. **37**, 673 (1983).
[39] A. Zvezdin, G. Vorobiov, A. Kadomtseva, Y. Popov, A. Pyatakov, L. Bezmaternykh, A. Kuvardin, and E. Popova, JETP Lett. **83**, 509 (2006).
[40] A. Zvezdin and V. Kotov, *Modern Magnetooptics and Magnetooptical Materials* (CRC Press, Boca Raton, 1997).
[41] A. Zvezdin, V. Matveev, A. Mukhin, and A. Popov, *Rare Earth Ions in Magnetically Ordered Crystals* (Nauka, Leningra, 1985), in Russian.
[42] M. N. Popova, T. N. Stanislavchuk, B. Z. Malkin, and L. N. Bezmaternykh, Phys. Rev. B **80**, 195101 (2009).
[43] A. I. Popov, D. I. Plokhov, and A. K. Zvezdin, Phys. Rev. B **87**, 024413 (2013).
[44] Y. A. Izyumov, R. P. Ozerov, and V. E. Naish, *Neutron Diffraction of Magnetic Materials* (Springer, Berlin, 1991).
[45] J. F. Dillon, J. Appl. Phys. **29**, 539 (1958).
[46] A. H. Eschenfelder, *Magnetic Bubble Technology* (Springer-Verlag, Berlin/Heidelberg/New York, 1981).
[47] A. Malozemoff and J. Slonczewski, *Magnetic Domain Walls in Bubble Materials: Advances in Materials and Device Research* (Academic press, New York, 2013), Vol. 1.